Volume 7 | Number 5 | 7 March 2023

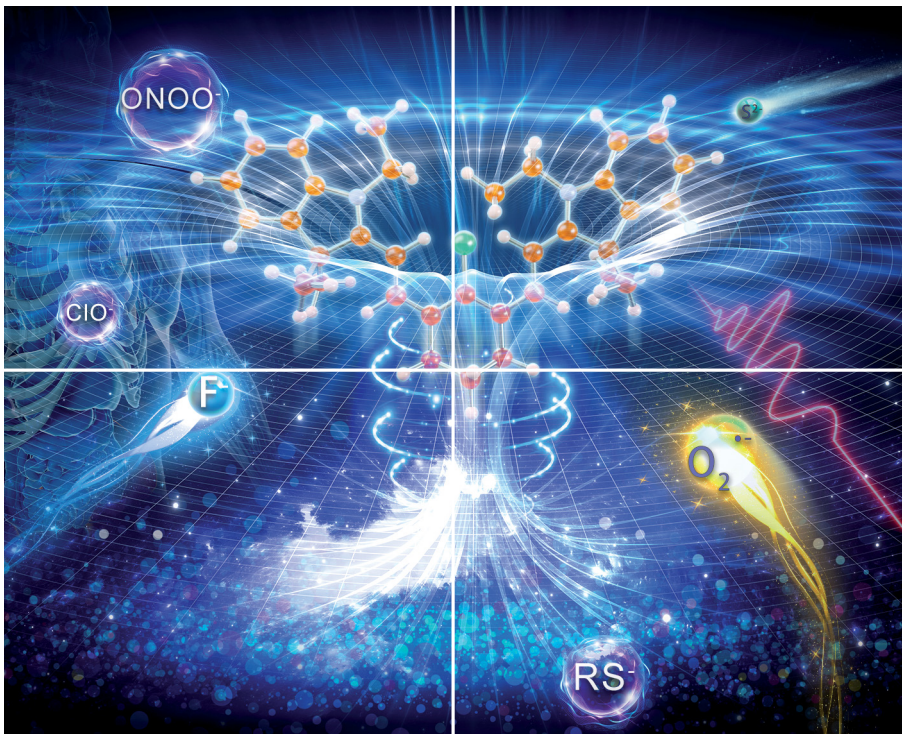

MATERIALS CHEMISTRY

FRONTIERS

CCS 中国化学会 CHINESE CHEMICAL SOCIETY
ICCAS
ROYAL SOCIETY OF CHEMISTRY
rsc.li/frontiers-materials

MATERIALS CHEMISTRY FRONTIERS

REVIEW

View Article Online
View Journal | View Issue

Cite this: *Mater. Chem. Front.*, 2023, **7**, 775

Activatable organic photoacoustic probes for *in vivo* anion imaging

Yurong Liu, † Xinming Zhang, † Shan Lei, Jing Lin * and Peng Huang *

Received 21st November 2022,
Accepted 12th December 2022

DOI: 10.1039/d2qm01207c

rsc.li/frontiers-materials

The merits of non-invasiveness, non-ionization and impressive tissue penetration depth of photoacoustic (PA) imaging technology make it attractive for *in vivo* detection. Analyte-responsive organic PA probe-based *in vivo* imaging of bio-functional small anions shows advances in real-time visualization of biological action, early diagnosis and precision therapy of diseases, due to the significance of such anion species in various physiological and pathological processes. In this mini review, the anion-recognition mechanisms of PA probes are particularly focused, from the perspective of chemistry, to exemplify the structural design strategies of activatable organic PA probes. Finally, the challenges and outlooks are discussed to pave the way for further development of PA probes for *in vivo* imaging of bio-functional small anions, which provides an alternative approach to interpret anion-mediated biological events.

1. Introduction

Bio-functional small anions have attracted broad attention recently due to their important roles in various physiological and pathological processes. For instance, fluoride ions (F^-) are closely related to osteoporosis and some dental diseases.[1–3] Reactive oxygen, nitrogen, and sulfur anion species (RONSs and RSSs), such as superoxide anions ($O_2^{\bullet -}$), hypochlorite (HClO/ClO^-), peroxynitrite ($ONOO^-$), and thiolates (RS^-), show significance in redox homeostasis and signal transduction in the living body.[4] Their overproduction results in oxidative or nitrosative stress, which disrupts intracellular redox homeostasis and further affects gene transcription, cellular signaling, the activity of various enzymes and bio-macromolecules, and the functionality of cells and organs. Oxidative stress could lead to free radical overaccumulation and further produce oxidative damage by lip peroxidation and oxidative modification of proteins.[5] Prolonged cellular or tissue damage may induce

Marshall Laboratory of Biomedical Engineering, International Cancer Centre, Laboratory of Evolutionary Theranostics (LET), School of Biomedical Engineering, Shenzhen University Medical School, Shenzhen, 518060, China.
E-mail: jingl@szu.edu.cn, peng.huang@szu.edu.cn
† Equal contribution.

Yurong Liu

Yurong Liu received her BSc in Polymeric Materials and Engineering (Sun Yat-sen University) and PhD in Chemistry (Hong Kong Baptist University) in 2014 and 2018, respectively. After graduation, she worked as a joint postdoctoral researcher at the University of Science and Technology of China (USTC) and Shenzhen University (SZU). Then she joined the Laboratory of Evolutionary Theranostics (LET) at SZU as an associate researcher. Her research interests focus on the design and synthesis of activatable organic materials for biomedical applications including diagnosis, treatment, and theranostics.

Xinming Zhang

Xinming Zhang received his doctorate degree in total synthesis of natural products at Paris-Sud, Paris-Saclay University, France in 2019. Then he worked with Prof. Jing Lin in the Laboratory of Evolutionary Theranostics (LET) at Shenzhen University (SZU) as a postdoctoral fellow. His current research focuses on the design and synthesis of activatable multimodal imaging probes to dissect pathological processes in vivo.

severe diseases such as cancers and cardiovascular diseases.[6] Therefore, cellular redox homeostasis is indispensable for maintaining the functioning of bio-macromolecules and cells. In this context, it is worthwhile to specifically detect these bio-functional anion species *in vivo*, which could afford plenty of vital information for the evaluation of the redox status of tissues.[7] Moreover, an *in vivo* anion imaging approach could be utilized for imaging of oxidative tissue injury or tumor imaging.[8,9] *In vivo* imaging of these anion species could make a complementarity with *in vitro* detection to elucidate the bio-functions of anions and acquire a comprehensive understanding of biological events, assisting in the theranostics and prognosis of diseases.[10]

To date, several optical[11–13]/non-optical[14,15] detection technologies, *e.g.*, positron emission tomography (PET), computed tomography (CT), ultrasound imaging (US), magnetic resonance imaging (MRI), and fluorescence imaging (FI) have been widely used for *in vivo* imaging. However, PET and CT are based on ionizing radiation, which increases the risk of radiation damage. US affords deep tissue penetration but is subject to low imaging resolution and contrast. MRI modality is much more expensive and unavailable for implant-carrying patients. The popular FI features excellent sensitivity and specificity, gratifying resolution and biological safety yet still suffers from serious light scattering of tissues, which causes undesirable signal interference and consequent low contrast and shallow imaging depth. By contrast, emerging photoacoustic imaging (PAI) is a promising technology, which collects ultrasound signals after light excitation. It combines optical and ultrasound technologies to achieve deep tissue penetration and, meanwhile, a satisfactory spatiotemporal resolution for *in vivo* imaging.[16,17] Furthermore, PAI could cooperate with other detection technologies to realize multimodal imaging as well as obtain qualitative or quantitative information on varying scales in a more accurate approach.[18–20] On the basis of this background, much effort has been devoted to the development of PA contrast agents, especially analyte-specifically responsive PA probes.[21,22] This kind of activatable PA probe displays signal variations after interaction with a specific analyte, showing the merits of excellent selectivity and a higher signal-to-noise ratio (S/N) than non-responsive PA contrast agents, due to the low background interference.[23,24] According to the varying signal outputs, this type of activatable PA probe could be divided into turn-on, turn-off and ratiometric types. After interacting with analytes, turn-on/off probes exhibit an intensity increase/decrease at the wavelength of the maximum PA signal. The turn-on/off times are used to appraise the amplitude of the signal changes. By contrast, ratiometric probes show signal peak shifts, by which the background interference is diminished instinctively.[25] Besides the single-stimulus activatable PA probe, dual- and even multi-stimuli responsive probes are attractive due to the less immature response interference.[26] An ideal activatable PA probe should have high absorptivity (molar extinction coefficient $> 10^4\ M^{-1}\ cm^{-1}$) in the first and second windows of the near-infrared (NIR-I and II) region avoiding the interruption of tissue and water, as well as possess a low quantum yield, excellent photothermal conversion ability and distinguished biological characteristics.[23,27,28] It seems a feasible shortcut to design PA probes from the existing NIR fluorescent (NIRF) probes, and there are indeed many successful examples. In the meantime, more factors should be carefully weighed up in a balanced manner. For instance, the fluorescence quantum yield, theoretically, should be low to intensify the nonradiative energy dissipation and then generate an amplified PA signal. Whereas a long-lived first excited state (S_1) with a high quantum yield conversely facilitates PA generation. Besides, the rotatable bonds within the probe could also improve PA emission by promoting nonradiative energy dissipation. For example, there is not any measurable PA signal detected from the classic fluorescent dyes methylene blue and

Jing Lin

Jing Lin is a Distinguished Professor at the School of Biomedical Engineering, Shenzhen University Health Science Center, China. She received her PhD in Organic Chemistry from the Donghua University and Shanghai Institute of Organic Chemistry, Chinese Academy of Sciences, in 2010. After two years, she moved to the United States of America and spent 4 years as a postdoc at the University of Maryland and the National Institutes of Health (NIH). She joined the faculty of Shenzhen University (SZU) in 2016 and was promoted to Distinguished Professor in 2018. Her research focuses on molecular imaging, nanomedicine and theranostics.

Peng Huang

Peng Huang is a Distinguished Professor, the Chief of the Laboratory of Evolutionary Theranostics (LET), and the Director of the Department of Molecular Imaging, at the School of Biomedical Engineering, Shenzhen University Health Science Center, China. He received his PhD degree in Biomedical Engineering from Shanghai Jiao Tong University in 2012. He then joined the Laboratory of Molecular Imaging and Nanomedicine (LOMIN) at the National Institutes of Health (NIH) as a postdoctoral fellow. In 2015, he moved to Shenzhen University as a Distinguished Professor. His research focuses on molecular imaging, nanomedicine and theranostics.

Rhodamine800 due to the lack of rotatable bonds.[29,30] Other parameters including excited state absorption, triplet state contributions, relaxation kinetics, solubility, and photobleaching[31–33] likewise affect the PA signal amplitude. Consequently, it remains challenging to design a well-performed PA probe.

The fundamental photophysical characteristics and typical structure of PA contrast agents can be found elsewhere[28,30,34] and will not be discussed in detail herein. The categories and various applications of PA probes have also been reviewed a lot.[17,31,35–38] Recently, Pu[39] and Chan *et al.*[40] gave overviews individually, focusing on PA probes for either different tissue imaging or tumor microenvironment profiling, highlighting the assembling methods and the performance of the nanoprobes. Tang *et al.* discussed the assembly strategies of organic dyes for FI and PAI.[41] However, there is no review article yet, to the best of our knowledge, systematically summarizing the recent development of activatable organic probes for *in vivo* anion imaging, and focusing more on the specific anion-recognition mechanisms of the probes at the molecular level. On the other hand, as aforementioned, *in vivo* anion imaging is of significance to early diagnosis and therapy of various diseases, and PAI shows unique superiority for *in vivo* imaging, which together causes an increasing number of original research papers published on the topic. Herein, we review the state-of-the-art studies to highlight the interactions between bio-functional anion species and activatable organic PA probes from the perspective of chemistry. The involved imaging mechanisms include cleavage, ring-opening, oxidation, degradation, substitution, and reduction reactions and the deprotonation process (Fig. 1). This review aims to imply future perspectives of this field to promote the extensive development of this kind of scarce PA probe.

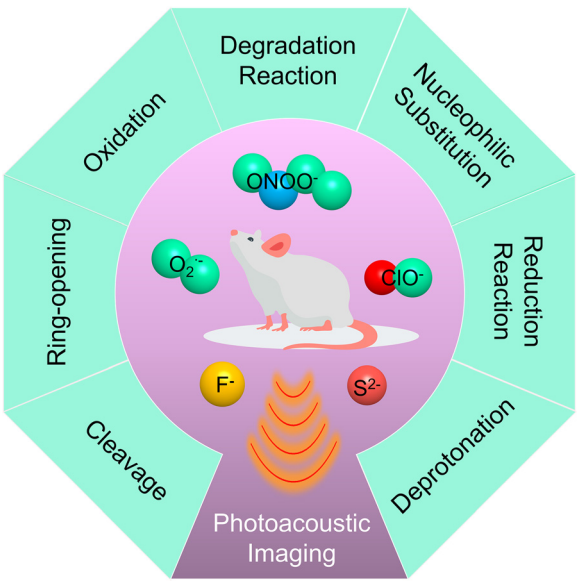

Fig. 1 An overview of activatable organic PA probes for *in vivo* anion imaging, with an emphasis on activation mechanisms.

2. Activatable organic PA probes for *in vivo* anion imaging

Essentially, the anion-recognition process mainly involves the specific analyte-induced chemical structural variation of the probe, further resulting in the change of their photo-chemical and -physical properties (*e.g.*, the aggregation state, charge transfer pathway), followed by the switch of the PA signal. In this section, the specific recognition mechanisms of activatable PA probes to bio-functional anion species are elaborately exemplified to clarify the probe design strategies.

2.1 *In vivo* imaging of reactive oxygen and nitrogen anion species

RONSs and RSSs are significant for redox homeostasis in all living systems. RONSs are highly active bio-oxidants. Among them, ionic RONSs $O_2^{\bullet-}$, $ONOO^-$, and $HClO/ClO^-$ are moderately unstable, with lifetimes of milliseconds or longer, and amenable to measurement. Moreover, they also show higher hydrophilicity than the lipophilic RONS-like singlet oxygen ($^1O_2$) and hydrogen peroxide (H_2O_2). Therefore, rational nanoengineering of PA probes could improve the selectivity towards these longer-lived polar RONSs.[42] Several activatable organic PA probes for imaging of these ionic RONSs are summarized in Table 1. The mechanisms include (i) cleavage; (ii) intramolecular spirolactone ring-opening; (iii) oxidation; and (iv) degradation reaction of PA probes towards ionic RONSs.

2.1.1. Cleavage

Ratiometric probes. It is believed that $O_2^{\bullet-}$ is the precursor of many other ROSs. This reactive species can lead to the cleavage of specific covalent bonds to induce structural changes. In this context, an $O_2^{\bullet-}$-responsive semiconductor polymer nanoprobe (RSPN) was developed by Zhang *et al.* It consisted of $O_2^{\bullet-}$-responsive molecules (ORMs), $O_2^{\bullet-}$-inert semiconducting polymers (OIMs), and amphiphilic polymers (DSPE-PEG_{2000}).[43] After being attacked by $O_2^{\bullet-}$, the trifluoromethanesulphonyl group in the ORM skeleton was cleaved, and then the ORMs could offer a robust "turn on" signal at around 690 nm, while a negligible change was observed at 800 nm which could be attributed to OIMs (Fig. 2a and b). Notably, the PA signal showed the same variation trend with absorption spectra (Fig. 2c), and the ratio of PA_{690}/PA_{800} exhibited a good linear relationship with the concentration of $O_2^{\bullet-}$. With respect to the selectivity, RSPN enables the specific differentiation of $O_2^{\bullet-}$ from other common reactive species such as H_2O_2, ·OH, NO_2^-, NO, $ONOO^-$, HClO, Cys, Hcy, and S^{2-}. Therefore, the ratiometric PAI (PA_{690}/PA_{800}) endowed RSPN with reliable visualization of $O_2^{\bullet-}$, which provided a noninvasive and high target-to-background ratio tool for examination of atherosclerotic plaque, in particular, for atherosclerotic complicated with pneumonia (Fig. 2d).

As a rapid reaction product of $O_2^{\bullet-}$ and NO, $ONOO^-$ also has strong oxidizing ability to break chemical bonds. For instance, Pu's group reported two PA probes to settle scientific problems of $ONOO^-$ sensing. One of them is the bulky borane-doped organic semiconducting nanoprobes (OSN-B1) constructed *via*

Table 1 Summary of the representative activatable organic PA probes for *in vivo* imaging of anions

Probe	Ion species	Reaction site	Mechanism	PA signal	Times turn-on (*in vivo*)	LOD	Animal model	Dose ($\times10^{-3}$ mg)/ injection method	Cytotoxicity (MTT assay)	Ref.
RSPN[db]	$O_2^{\bullet-}$	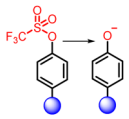	Cleavage	PA_{690}/ PA_{800}	—	—	Plaque-bearing mice (with or without pneumonia)	14 *i.v.*	40 μg mL^{-1} (ORM)	43
OSNs[db]	$ONOO^-$	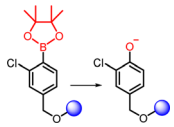	Cleavage	PA_{745}/ PA_{675}	2.6-fold	100 nM	4T1 xenograft tumor	25 *i.v.*	100 μg mL^{-1}	44
$CySO_3CF$[ea]	$ONOO^-$	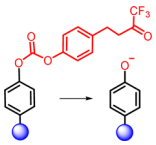	Cleavage	PA_{680}	2.1-fold	145 nM	4T1 xenograft tumor	3.8 *i.v.*	80 μmol L^{-1}	45
PA-MMSiNQ[da]	HOCl	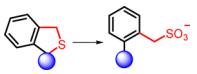	Spirolactone ring-opening	PA_{660}	—	—	Mouse thigh	2.9 *s.c.*	—	46
SiRho-HD[ec]	$ONOO^-$	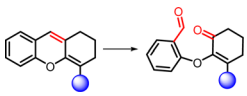	Oxidation	PA_{715}	—	1.3 μM	Acute kidney injury	10.5 *i.v.*	10 μM	47
BDP-DOH[db]	$O_2^{\bullet-}$	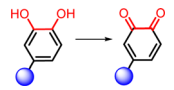	Oxidation	PA_{750}/ PA_{680}	6.3-fold	30 nM	EMT6 xenograft tumor	10 *i.v.*	100 μg mL^{-1}	48
ONc/IR780 @F127[db]	$ONOO^-$	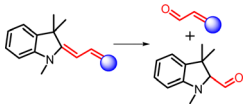	Degradation	PA_{860}/ PA_{775}	2.34–2.22-fold (tumor *vs.* thigh)	10 nM	4T1 xenograft tumor and thigh	25 (ONc) *i.v.*	10 μg mL^{-1} (ONC)	49
SOA[db]	ClO^-	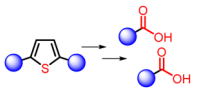	Degradation	PA_{780}/ PA_{680}	1.47-fold (6 h *vs.* 2 h post-injection)	700 nM	4T1 xenograft tumor	50 *i.v.*	50 μg mL^{-1}	50
NIR-S[eb]	Cys/ Hcy	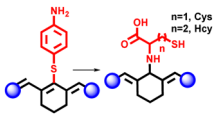	Nucleophilic substitution	PA_{695}/ PA_{840}	> 10-fold	—	Leg	4.6 *i.v.*	50 μM	54
ZNNPs[eb]	H_2S	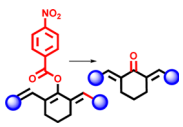	Nucleophilic substitution	PA_{680}/ PA_{900}	2.8-fold	0.68 μM	Acute hepatoxicity, cerebral hemorrhage, HCT116 xenograft tumor	10 mg kg^{-1} *i.v.*	100 μg mL^{-1}	57
AzHD-LP[db]	H_2S	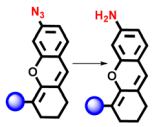	Reduction	PA_{700}/ PA_{532}	—	91 nM	HCT116 xenograft tumor	1 mg kg^{-1} *i.v.*	100 μg mL^{-1}	58
LET-1[da]	F^-	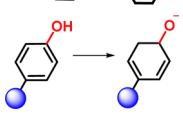	Deprotonation	PA_{680}	4-fold	0.2 mM	Mouse liver	40 μM, *s.c.*/ 5 mg kg^{-1}, *i.v.*	—	63

Note: The response type: [a] Turn on. [b] Ratiometric. [c] Turn off. [d] PA imaging. [e] PA/FL dual-model imaging. Fold turn-on: PA intensity enhancement of the probe-treated group *versus* control group (unless otherwise specified). LOD: the limit of detection. Model: mouse. Injection methods: *i.v.*: intravenous injection; *s.c.*: subcutaneous injection; and *i.c.*: co-incubation.

nanoprecipitation *via* the assistant of an amphiphilic polymer, PEG-*b*-PPG-*b*-PEG for ratiometric PAI of $ONOO^-$ in real-time (Fig. 2e).[44] Both nanoprobes consist of a boronate-caged boron-dipyrromethene dye (BBD) as the primary $ONOO^-$-responsive

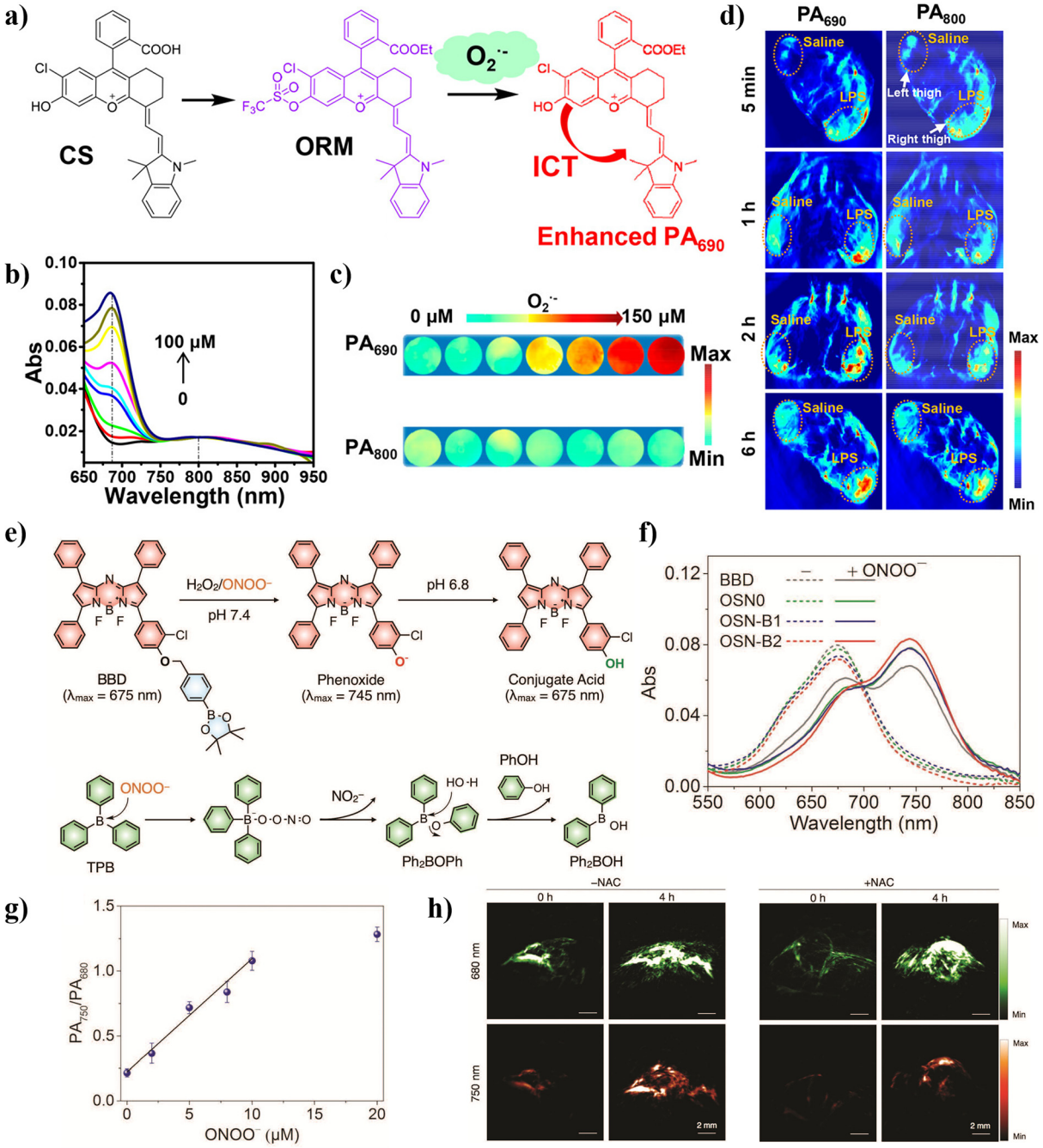

Fig. 2 (a) Chemical structure of ORMs and the responsive mechanism of ORMs to $O_2^{\bullet-}$; (b) absorption spectra and (c) PA images at 690 or 800 nm of RSPN upon addition of $O_2^{\bullet-}$ in PBS; (d) PA images of the LPS-stimulated acute inflammation mice model; (e) chemical structure and reaction mechanisms of BBD and bulky borane (TPB); (f) absorption spectra of OSNs and BBD after addition of $ONOO^-$; (g) PA_{750}/PA_{680} of OSN-B1 as a function of the concentration of $ONOO^-$; (h) *in vivo* ratiometric PAI of $ONOO^-$. (a–d) Reprinted (adapted) with permission from ref. 43, Copyright 2021, American Chemical Society; (e–h) reprinted (adapted) with permission from ref. 44, Copyright 2016, Wiley-VCH Verlag GmbH & Co. KGaA.

molecule, which could undergo the breakage of an ether bond to recover the intramolecular charge transfer process. To get around the unspecific response of the BBD toward both $ONOO^-$ and H_2O_2, an $ONOO^-$-degradable but H_2O_2-inert shield triphenylborane (TPB) was ingeniously doped to prevent the BBD from reacting with H_2O_2. Initially, the absorption spectra of the probe showed a maximum absorption peak at 675 nm. With the addition of $ONOO^-$, the absorption at 675 nm was reduced gradually, accompanied by the emergence of a new peak at 745 nm (Fig. 2f). At the saturation point, the absorbance ratio (Ab_{745}/Ab_{675}) of the OSNs was ~1.7, which was 8-fold higher than that of the initial state (0.21) (Fig. 2g). The activation of probes could be explained by $ONOO^-$, which caused rapid oxidative cleavage of the borate ester moiety of the BBD.

The formed anionic phenoxide product showed a characteristic absorption peak at 745 nm. Furthermore, there was no absorption change of the probes in response to other ROSs, indicating their high selectivity in the presence of $ONOO^-$. Finally, the nanoprobes were successfully applied for ratiometric PAI of $ONOO^-$ in 4T1 xenograft tumor-bearing mice (Fig. 2h).

Turn-on probes. The co-assembly of two components often suffers from complicated synthesis procedures and the risk of pre-leakage. Later, the same research group explored a molecular probe ($CySO_3CF_3$) with good water solubility, used for *in vivo* NIRF/PA dual-modal imaging of $ONOO^-$. It contains a trifluoromethyl ketone moiety (TFK), an $ONOO^-$-sensitive unit, and a caged hemicyanine dye with a zwitterionic structure (Fig. 3a).[45] It could only be activated by $ONOO^-$ among various RONSs such as H_2O_2,·OH, $^1O_2$, and ClO^-. In the presence of $ONOO^-$ and $CySO_3CF_3$ was cleaved into the uncaged structure ($CySO_3OH$), undergoing a series of cascade oxidation–elimination reactions, accompanied by changes of absorption spectra (Fig. 3b) as well as the emergence of the PA signal. Then 4T1 tumor-bearing mice were systemically administered with $CySO_3CF_3$ for PAI of $ONOO^-$ and the PA intensity in the tumor region was 2.1-fold higher than that of the control (Fig. 3c).

2.1.2. Ring-opening

Turn-on probes. By virtue of the ROS-induced spirocycle opening of rhodamine, Urano's group developed a ROS-responsive PA probe, namely, PA-MMSiNQ (silicon-rhodamine based NIR scaffold) by the aforementioned spirocyclization strategy for *in vivo* detection of HOCl.[46] The "closed" spirolactone probe PA-MMSiNQ is transparent in the NIR region, yet a significant absorption at 660 nm was observed in the presence of HOCl (S/N > 70), due to the ring-opening reaction following the oxidation of the sulfur atom (Fig. 4a and b). PA-MMSiNQ also showed high selectivity to HOCl against other ROSs. Finally, 3D PAI of HOCl in mouse subcutis was successfully realized by the activatable PA probe (Fig. 4c).

2.1.3. Oxidation

Turn-off probes. Owing to the strong oxidizing ability of RONSs, electron donors such as O, S, N, Se, Te, and olefin groups within aromatic systems get easily oxidized as carbonyl derivatives by such reactive anions. Based on this result, Zhang's group built a ratiometric NIRF/PA dual-modal imaging probe SiRho-HD to monitor the fluctuation of $ONOO^-$ in cisplatin-induced acute kidney injury.[47] SiRho-HD contains HD and Si-Rho two units with absorption peaks at 660 and 719 nm, respectively. With the addition of $ONOO^-$, the absorption of SiRho-HD at 719 nm was gradually reduced until it disappeared due to the oxidative destruction of the xanthene scaffold. Similarly, the PA signal at 715 nm exhibited a 3.9-fold decay at the saturation point with the addition of $ONOO^-$. Although negligible PA signal fluctuation was observed from most RONSs, HOCl showed some interference on the recognition of $ONOO^-$ under acidic conditions.

Ratiometric probes. Based on a similar mechanism, Zhang's group synthesized a reversibly activatable PA molecule, BDP-DOH, which consisted of an NIR boron dipyrromethene (BODIPY) dye, to evaluate the *in situ* redox status of tissues *in vivo* by tracing the redox circulation of $O_2^{\bullet-}$ and GSH (Fig. 5a).[48] When $O_2^{\bullet-}$ was encountered, the *ortho*-phenolic hydroxyl unit on BODIPY could be easily and specifically oxidized, and consequently the probe absorption at 680 nm was diminished while that at 750 nm was conversely enhanced (Fig. 5b), leading to an increased ratio of PA_{750}/PA_{680} (Fig. 5c). When $O_2^{\bullet-}$ was added, a 9.84-fold enhancement of the PA_{750}/PA_{680} ratio of BDP-DOH was recorded. However, little variation of the ratio was observed after the addition of other RONSs. Then, a nanoprobe BDP-DOH/LP was assembled with BDP-DOH and an amphiphilic lipid (LP), DSPE-PEG_{2000}-COOH, to

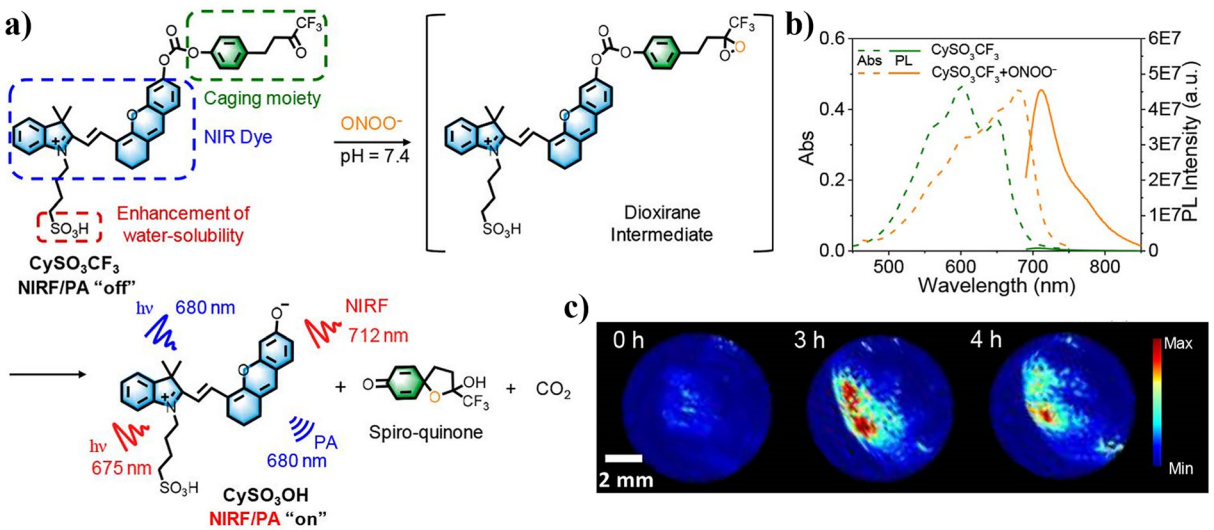

Fig. 3 (a) Chemical structure and sensing mechanism of $CySO_3CF_3$ to $ONOO^-$; (b) UV-vis absorption (dashed line) and fluorescence (solid line) spectra of $CySO_3CF_3$ in the absence or presence of $ONOO^-$; (c) representative PA imaging projection of tumors from a systemic administration of a living mouse at 0, 3, and 4 h post-injection of $CySO_3CF_3$. Reprinted (adapted) with permission from ref. 45, Copyright 2018, American Chemical Society.

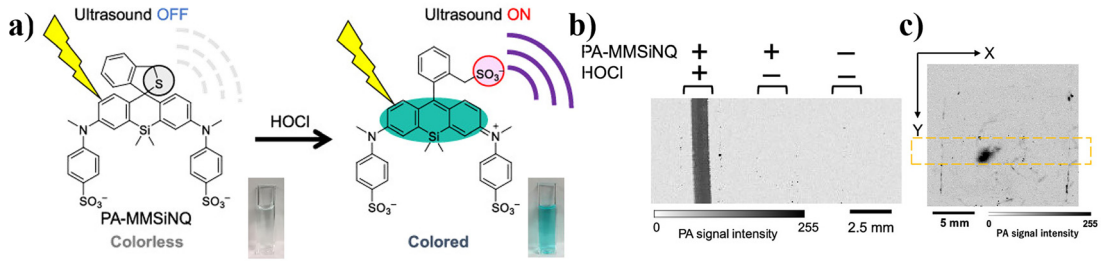

Fig. 4 (a) Chemical structure and sensing mechanism of PA-MMSiNQ for HOCl; (b) PA image of PA-MMSiNQ after (left) and before (middle) reaction with HOCl in PBS and PBS only (right); (c) PA images in living mice. Reprinted (adapted) with permission from ref. 46, Copyright 2019, American Chemical Society.

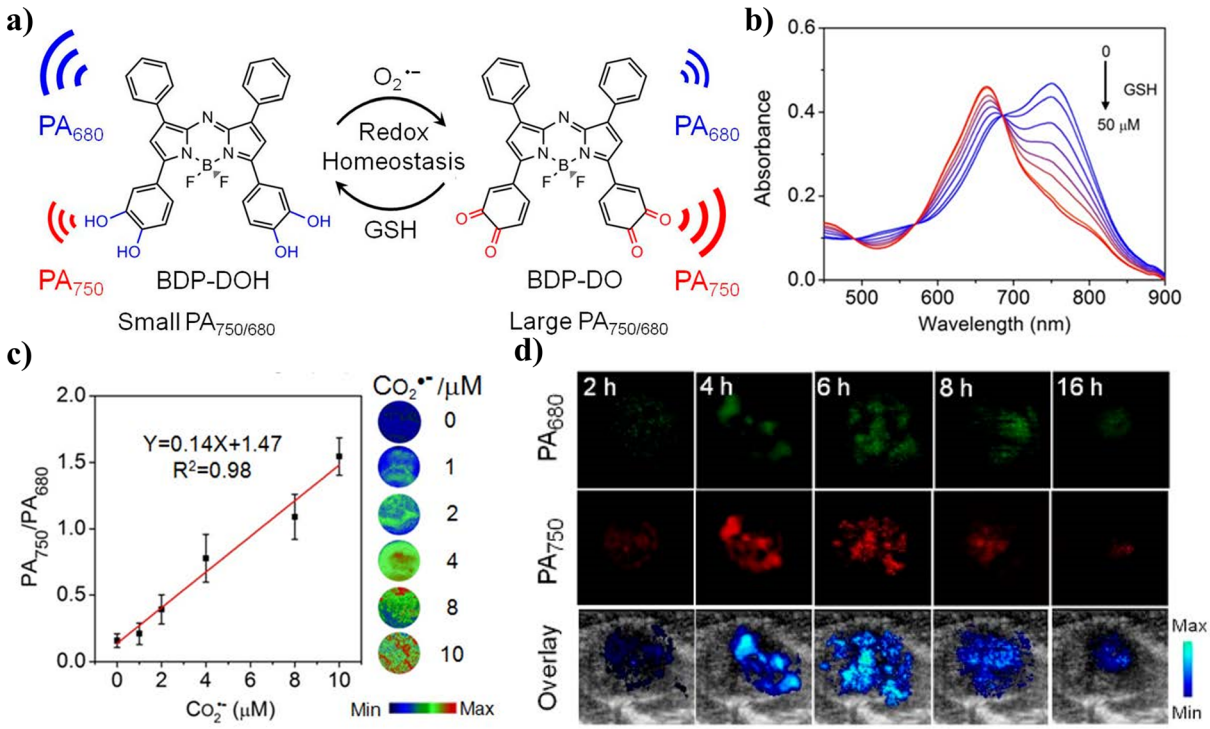

Fig. 5 (a) Chemical structure and the reversible PA sensing mechanism of BDP-DOH towards $O_2^{\bullet-}$ and GSH; (b) absorbance changes of BDP-DOH upon titration with $O_2^{\bullet-}$; (c) the PA_{750}/PA_{680} intensity of BDP-DOH with different concentrations of $O_2^{\bullet-}$; (d) real-time PA and US (grey) images of the redox status in the tumor-bearing mouse pre-treated with PMA. Reprinted (adapted) with permission from ref. 48, Copyright 2019, American Chemical Society.

optimize the biological characteristics of BDP-DOH and to facilitate the delivery into tumor tissues *via* the improved permeability and retention effect (Fig. 5d).

2.1.4. Degradation

Ratiometric probes. Degradation of PA probes usually leads to signal attenuation, which thereby displays an undesirable turn-off PA response to analytes. To overcome the obstacle, an inert reference compound can be co-assembled with the responsive probe *via* nano-engineering to achieve the ratiometric PA signals towards specific target analytes. Naphthalocyanine is a commonly used NIR reference dye due to its excellent stability towards RONSs. Lin's group fabricated such a ratiometric PA nanoprobe which contained an $ONOO^-$-sensitive IR780 iodide dye and an $ONOO^-$-inert internal standard, 5,9,14,18,23,27,32,36-octabutoxy-2,3-naphthalocyanine (ONc) (Fig. 6a).[49] With the addition of $ONOO^-$ into the probe solution, the PA signal at 775 nm declined due to the $ONOO^-$-induced oxidative degradation of IR780 (Fig. 6b), while that of ONc at 860 nm remained nearly unchanged. Moreover, the PA_{860}/PA_{775} ratio of the probe was ~2.88 in response to $ONOO^-$, while they were less than 1.5 for other RONS analogues and RSSs (NO^-, ClO^-, $O_2^{\bullet-}$, H_2O_2, ROO·, ·OH, $^1O_2$, Cys, Arg), exhibiting high selectivity. After intratumoral injection of the nanonaps, the PA_{860}/PA_{775} ratio of tumor tissues gradually rose up to 3.10 ± 0.084 at 120 min-post-injection, while that of the control group remained almost unvaried (1.36 ± 0.001) within 120 min

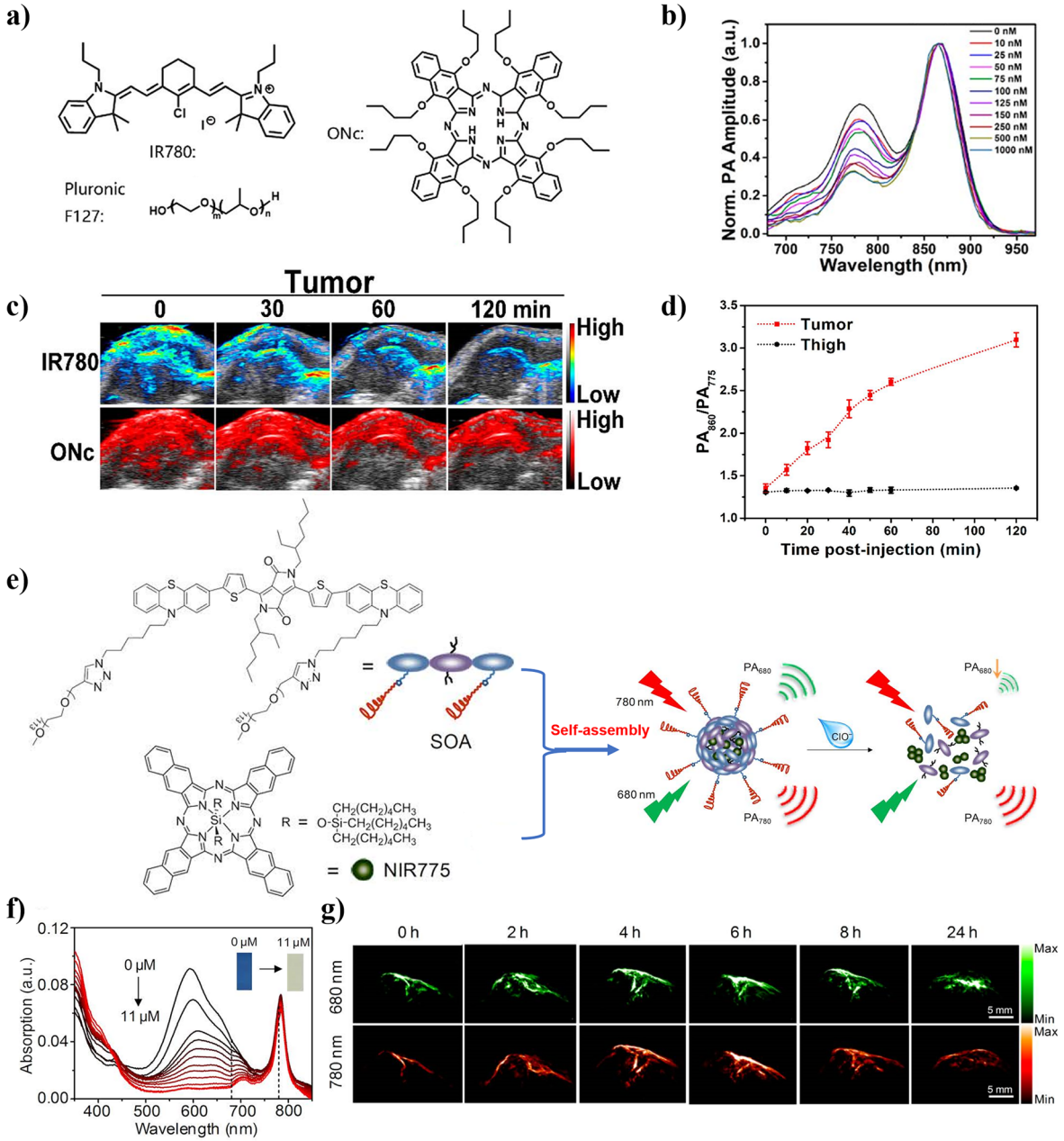

Fig. 6 (a) Chemical structures of IR780, pluronic F127, and ONc used for the preparation of nanonaps; (b) PA spectra of nanonaps with different concentrations of $ONOO^-$; (c) *in vivo* ratiometric PAI performance of the nanonaps to $ONOO^-$ in 4T1 tumor tissues; (d) PA_{860}/PA_{775} ratios as a function of post-injection time; the chemical structures of the SOA and NIR775 used for the synthesis of the PA nanoprobe *via* a self-assembly process and illustration of the sensing mechanism for the nanoprobe; (f) UV-vis absorption spectra of the nanoprobe upon addition of ClO^-; (g) representative PA image of a subcutaneous 4T1 tumor in a nude mouse. (a–d) Reprinted (adapted) with permission from ref. 49, Copyright 2018, American Chemical Society; (e–g) Reprinted (adapted) with permission from ref. 50, Copyright 2017, American Chemical Society.

post-injection, achieving the ratiometric imaging of $ONOO^-$ *in vivo* (Fig. 6c and d).

Similarly, Pu and co-workers utilized stimulus-responsive semiconducting polymers to construct diverse analyte-responsive PA probes for the ratiometric detection of biomarkers *in vivo*. Among them, a PA nano-platform for the *in vivo* detection of ClO^- was constructed with a semiconducting polymer (SOA) as the responsive component and the NIR775 dye as the inert reference (Fig. 6e).[50] In the presence of ClO^-, the characteristic absorption of SOA at 596 nm attenuated gradually due to the ClO^--caused oxidative degradation of the probe, while the absorbance at 784 nm (assigned to NIR775) remained constant (Fig. 6f). The spectral variation of the nano-platform afforded the quantitative analysis of ClO^- based on the comparative analysis of the ratio of the absorbances at 780 and 680 nm (Ab_{780}/Ab_{680}). In good agreement with the absorption spectra, the PA_{780}/PA_{680} value of the nanoprobe in response to ClO^- was 8.3-fold higher than that in the initial

inactivated state. After systemic administration of the nanoprobe in tumor-bearing mice, the ratiometric PA signals ($\Delta PA_{780}/\Delta PA_{680}$) in tumors were increasing over time and peaked at 6 h post-injection, which was ~1.47-fold stronger than that at 2 h post-injection, thus verifying the capability of the probe as a highly sensitive PA indicator of ClO^- in the tumors of a living mouse (Fig. 6g).

In summary, the recognition of ionic RONSs is primarily based on the oxidation reaction of the probes, though the presented final structural transformation varies. For instance, probes containing an aromatic sulphonyl group, borate ester, or carbonic ester are prone to be cleaved to form phenol anion analogues by oxidation. The ring-closed rhodamine precursor is a typical response group of RONSs *via* a ring-opening mechanism. Moreover, the *para*-position of O within xanthene and the *ortho*-phenolic hydroxyl group are apt to be oxidized as carbonyl groups, while the cyanine skeleton is directly destroyed due to the oxidation of the polyene segment. In this context, the probe selectivity towards various RONSs may get improved by carefully considering the difference of these reactive species with respect to their oxidizing capability and then embedding the corresponding specific response moieties into the PA probes. Furthermore, nano-engineering of the probe to achieve a ratiometric PA signal may improve the S/N ratio and selectivity. For instance, by co-assembling with an inert reference, the formed ratiometric probe ONc/IR780@F127 displayed a low LOD of 10 nM toward $ONOO^-$ with good selectivity.

2.2. *In vivo* imaging of reactive bio-thiol species

In contrast to RONSs, RSSs usually function as bio-reductants. Moreover, there exists a wide variety of RSSs, such as thiols (GSH, Cys, homocysteine (Hcy)), SO_2, H_2S, and so on. The sulfhydryl anions (RS^-) are practically reactive,[51] therefore, thiolates are covered in this mini review, which focuses broadly on bio-functional ions. Several representative examples of PA probes for RS^- imaging are selected to illuminate the recognition mechanisms, which mainly include reduction and nucleophilic substitution reactions. These examples might inspire potential progress in the future.

2.2.1. Nucleophilic substitution reaction

Ratiometric probes. Among various RSSs, GSH, Cys, and Hcy have piqued researchers' significant interest as they are the most important bio-thiols. Significant research efforts have been devoted to detecting them.[52] For instance, specific responses to thiols can be realized through the interchange of the –S–S– and –SH groups within probes.[53] Therefore, disulfide motifs occupy an important position in thiol detection, and drug delivery and release systems. On the other hand, as the sulfhydryl anion (RS^-) is the practically reacting constituent of RSSs, its nucleophilic nature could be utilized for the activation of probes. For example, He's group reported a *para*-amino phenyl thioether-substituted cyanine dye probe NIR-S for NIRF and ratiometric PA dual-modal *in vivo* imaging of Cys and Hcy.[54] Basically, the aryl-thioether of NIR-S was subjected to nucleophilic attack by Cys/Hcy and it subsequently underwent the Smiles rearrangement reaction, leading to a turn-on NIR fluorescence and ratiometric PA response. With the addition of Cys/Hcy, the ratio of PA intensities at 695 nm (PA_{695}) and 840 nm (PA_{840}) showed a dramatic increase. Except for Cys and Hcy, other biologically relevant species including diverse amino acids, GSH, Na_2S, and other inorganic sulfur species (HSO_3^-, $S_2O_3^{2-}$, SO_4^{2-}) showed a negligible influence on both the emission and absorption of the probe, even when a high concentration of GSH was used. Furthermore, NIR-S was applied for the *in vivo* PAI of exogenous Cys/Hcy in the subcutaneous tissue of living mice. The PA_{695}/PA_{840} value of the control group was recorded to be 0.220, while that of the Cys-treated right hind limb boosted over 10 fold was found to be 1.406. However, most of the currently reported thiol-activated probes usually exhibit responses to both Cys and Hcy. In this context, the improvement in the selectivity of PA probes towards Cys over Hcy is urgently required. Moreover, it may be realized by modulating the electrophilic nature of the response site, considering that Cys shows the highest nucleophilic activity among the three thiols (GSH, Cys, and Hcy).[55]

H_2S (HS^-) is a key gasotransmitter involved in signalling pathways and pathogenesis.[56] As another typical RS-species with a much small particle size, it could be recognized by a similar nucleophilic reaction mechanism. Shi *et al.* reported such an H_2S-sensitive and consuming nanoplatform (ZNNPs) for the quantitative and real-time detection of endogenous H_2S.[57] ZNNPs and ZNNPs@FA were obtained by encapsulation of an H_2S-responsive hydrophobic NIR-II fluorophore ZM1068-NB in amphiphilic $mPEG_{5000}$-PCL_{3000} and $mPEG_{5000}$-PCL_{3000}-FA polymers, respectively (Fig. 7a). Based on the H_2S-reactive nucleophilic addition of a 4-nitrobenzoic ester of ZM1068-NB, the ZM1068-ketone product was released, concomitant with absorption and PA spectral shifts (Fig. 7b and c). The PA signal at 680 nm (PA_{680}) remained almost unchanged, while those at 900 nm (PA_{900}) gradually declined against the increasing concentration of NaHS with an LOD of 0.68 μM. Moreover, the ratiometric PA signals (PA_{680}/PA_{900}) of ZNNPs became significantly brighter with the addition of NaHS over other interferential anions (SCN^-, NO_3^-, SO_4^{2-}, NO_2^-, vitamin C, GSH, H_2O_2, CO_3^{2-}, $S_2O_3^{2-}$, and SO_3^{2-}, and AcO^-) and metal ions (K^+, Ca^{2+}, Na^+, Mg^{2+}). Next, a 2.25-fold enhancement of the PA_{680}/PA_{900} value was observed in the mice livers treated with 5 mM L-cys (a precursor for the biosynthesis of H_2S) relative to the liver of normal mice, indicating the potential for deeply penetrated imaging of H_2S-related diseases, such as acute hepato-toxicity, brain injury, and colorectal tumors (Fig. 7d).

2.2.2. Reduction reaction

Ratiometric probes. H_2S-initiated reduction of azide is another effective mechanism to design PA probes. Xing's group developed a novel nanoprobe AzHD-LP for switch-on ratiometric PA imaging of H_2S by encapsulation of an H_2S-sensitive moiety (AzHD) in a liposome (LP).[58] Induced by H_2S, the electron-withdrawing azide was reduced to an electron-donating amine, accompanied by a red-shift of the absorption peak of the AzHD-LP from 600 to 700 nm (Fig. 7e). Moreover, the ratio of PA_{700}/PA_{532} increased by 23 fold with the addition of NaHS from 0 to 100 μM. The LOD was then calculated to be 91 nM.

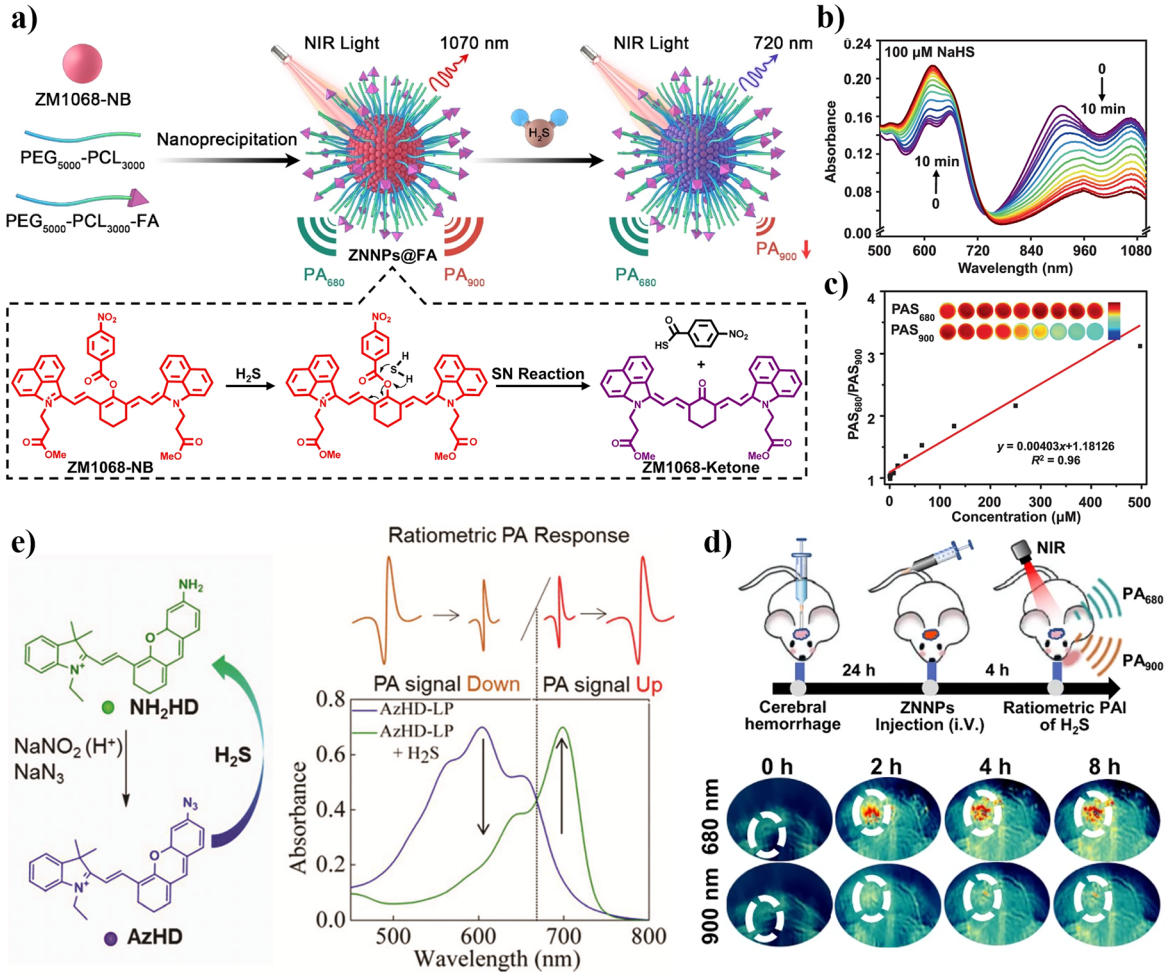

Fig. 7 (a) Schematic illustration of the fabrication of ZNNPs@FA and principle of quantitative visualization of H_2S; (b) normalized absorption of ZNNPs upon incubation with NaHS; (c) linear fitting of the PAS intensity of ZNNPs with various concentrations of NaHS; (d) schematic description of intracerebral hemorrhage (ICH) model construction and PA detection of endogenous H_2S by using ZNNP; (e) the proposed mechanism for the ratiometric photoacoustic detection of H_2S by using AzHD. (a–d) Reprinted (adapted) with permission from ref. 57, Copyright 2022, Springer Nature; (e) Reprinted (adapted) with permission from ref. 58, Copyright 2020, Science China Press and Springer-Verlag GmbH Germany, part of Springer Nature.

Moreover, it exhibited specific responses to NaHS among various biospecies such as SO_3^{2-}, CN^-, NO_3^-, OH^-, ClO_3^-, F^-, GSH and H_2O_2. For *in vivo* performance, the amount of H_2S in brain tissues of normal and AD mice was, respectively, monitored by the ratiometric PA probe. The ratio of PA_{700}/PA_{532} of the normal brain tissues was 6.5-fold higher than that of the control group, while that of the AD group only displayed 1.2-fold enhancement, describing the absence of H_2S in the AD mouse brain. Next, by covalent connection with a tumor targeted peptide c(RGDyK), AzHD-LP was also used as a ratiometric PA probe for intratumoral H_2S monitoring in real-time in an HCT116 tumor-bearing mouse model.

Overall, RSSs exhibit distinct characteristics from RONSs. FI detection of specific RSSs has been extensively explored based on intramolecular hydrogen bonding, aromatic nucleophilic substitution, and addition reactions.[59–61] By contrast, PA imaging of RSSs is still not fully developed, in particular, for PAI of Hcy. Besides, PA probes for *in vivo* imaging of selenols or thiophenols are scarce. Such PA probes may be acquired by using similar design strategies to that for imaging of GSH, Cys and HCy, as sulfhydryl anions are the dominantly reacting constituents.

2.3 Imaging of other anions

Except for the reactive anion species, the PA probe can also be utilized for *in vivo* imaging of F^-. Excessive F^- ingestion in the human body may seriously damage the hard tissues and renal system, leading to severe diseases such as dental or skeletal fluorosis, urolithiasis, and kidney failure.[62] Detection of F^- makes sense for precision diagnosis of diseases. On the other hand, F^- is the smallest anion, and therefore features a small radius to charge ratio, indicating high reactivity towards Lewis acid. The currently reported detection mechanisms mainly include Lewis acid–base interactions, such as the high affinity of F^- towards boron atoms, hydrogen-bonding interaction and breaking of the Si–O bond to alter the molecular orbital energy.

2.3.1. Deprotonation

Turn-on probes. Based on the chemical characteristics of F^-, PAI of F^- has been exemplified with a probe LET-1 reported by Lin's group.[63] LET-1 consisted of a naphthalimide unit as a chromophore and a phenol group as an F^--sensitive unit. Specifically, F^--induced deprotonation of LET-1 led to a red-shift of the light absorption from the visible 430 nm region to the NIR 640 nm region, thereby generating a PA signal at around 600 nm. The fluorescence emission at 600 nm was quenched, as the deprotonated LET-1@ exhibited a smaller highest occupied molecular orbital and the lowest unoccupied molecular orbital (HOMO–LUMO) band gap (E = 1.7762 eV) than LET-1 (E = 3.2873 eV). After the addition of F^- (80 mM), LET-1 displayed an over 20-fold enhancement of the PA intensity at 680 nm, with a detection limit of 0.20 mM. Besides, negligible changes were observed on the probe in response to various anions such as I^-, $H_2PO_4^-$, HCO_3^-, AcO^-, Cl^-, NO_2^-, CN^-, and SO_4^{2-}, indicating the good selectivity of LET-1 toward F^-. The *in vivo* PAI tests on mice showed a 4-fold intensity increase of PA_{680} after F^- administration, demonstrating the competence of LET-1 for *in vivo* F^- imaging.

3. Challenges and outlooks

The main text of the article includes activatable organic PA probe-mediated anion imaging, which is indeed significant for the *in situ* screening of pathological tissues like solid tumors as well as the visualization of physiological activities. However, the further development of PA probe-based anion imaging has still been hampered by the following three aspects: (1) the category of anion species, the *in vivo* imaging of which has been realized, remained unexpanded and the performance of the organic PA probes need to be improved; (2) quantitative detection methods are largely unexplored; and (3) instrumental limitations. Firstly, the reported organic PA probes for anion imaging are still inadequate, especially high-performance probes with excellent selectivity, sensitivity, and biocompatibility. It is also necessary to diversify the studied anion species, considering that there are much more anion species that participated in vital life processes in living systems. In addition, the accurate quantitative detection of anions is urgently required. As for the instrument, the optics (such as laser source) and electronics (such as detectors) are vital devices for PA imaging. To meet the requirements of preclinical or clinical applications, a portable and user-friendly instrument is much desirable, especially the hand-held type. However, the currently explored detectors are bulky and the laser source is much expensive, which is unfavourable for further development of PAI.[64–67] On the other hand, multispectral imaging is increasingly attractive for clinical application, which requires a pulse laser source with strong energy and optical parametric oscillators. The performance of the present laser source remains to be improved to fit the bill.[38]

Therefore, more effort could be devoted to either exploring the novel well-performed organic PA probes or modifying the existing molecules by elaborate structural design to optimize the performance. The investigation on the excited state absorption and the triplet contribution relaxation kinetics are helpful to reinforce the photothermal conversion efficiency. Besides, combination with other materials by engineering method is beneficial for improving the blood circulation time and stability of the probes. It is necessary to establish the relationship between the property and chemical structure. The photophysical properties (photostability, strong NIR-I even II region absorption), chemical capabilities (chemical stability, sensitivity, selectivity, and water-solubility, high photothermal conversion efficiency) as well as the biological characteristics (long blood circulation, targeting ability, low toxicity, biocompatibility, biodegradability) and economic cost should be comprehensively considered. For instance, the PA probes with NIR-II absorption and high absorption coefficients are expected to achieve high spatial resolution and excellent imaging contrast. Generally, the strong NIR absorption of PA probes is related to their large structural conjugation, which however may lead to high molecular rigidity, and consequently poor biocompatibility. In addition to the photophysical properties, the biological characteristics are also essential considerations as most of the organic PA probes are limited by their poor water solubility and rapid metabolism from the living body. Introducing the hydrophilic moieties into the skeleton to increase the solubility may inversely cause a reduced absorption intensity and hypochromic shift. Nano-engineered probes are usually excreted by the reticuloendothelial system. However, it increases the risk of organ toxicity due to excess enrichment of nanoprobes in the liver and spleen.[68] To reduce the safety concerns, renal-clearable PA probes have been increasingly explored, due to the minimal metabolism process and the accessibility to anion imaging of kidneys.[69] Furthermore, new detection methods or responsive mechanisms for optimal *in vivo* anion imaging are required. Quantitative detection and reversible imaging, which is necessary for dynamic monitoring, are lacking. Also, the challenges of the instrumental limitations of poor resolution, narrow dynamic range, and confined laser wavelength need to be addressed to better match the characteristics of probes and realize high resolution and contrast imaging outcomes. The technic parameters of both optics (*e.g.*, cost, pulse length and energy of laser source) and electronics (*e.g.*, sensitivity, size and array conformation of detectors) need to be optimized to promote the generalization of PAI.

4. Conclusions

The recent advances of such probes are summarized in this review, with a particular emphasis on specific anion-induced activation mechanisms of these PA probes at the molecular level. The anion-recognition of these PA probes involves diverse chemical reactions, mainly including cleavage, spirolactone ring-opening, oxidation, degradation, nucleophilic substitution, and reduction reactions, and the deprotonation process. On the basis of these mechanisms, the rational structural

design of the analyte-response unit of the activatable PA probes could be achieved to develop anion-responsive PA probes with excellent selectivity and sensitivity. Finally, the challenges and perspectives are also discussed. Much effort should be devoted to (1) developing high-performance anion-responsive organic PA probes by nanoengineering and/or the chemical modification approach, (2) innovating detection methods and (3) combining PAI with other imaging technologies to achieve multispectral, multimodal and multifunctional detection of anion species *in vivo*. In this way, activatable organic PA probes for *in vivo* imaging of bio-functional anion species, as an important part of the *in vivo* molecular imaging platform, hold great promise for unveiling the involved physiological and pathological secrets.

Abbreviation

AcO^-	Acetate ion
Arg	Arginine
CT	Computed tomography
Cys	Cysteine
cRGD	Tumor-targeting short peptide c(RGDfK)
DSPE-PEG_{2000}	1,2-Distearoyl-*sn-glycero*-3-phosphoethanolamine-*N*-[methoxy(polyethylene glycol)-2000]
DSPE-PEG_{2000}-COOH	1,2-Distearoyl-*sn-glycero*-3-phosphoethanolamine-*N*- [carboxy(polyethylene glycol)-2000]
F^-	Fluoride ion
FI	Fluorescence imaging
GSH	Glutathione
HClO/ClO^-	Hypochlorite
HOMO	Highest occupied molecular orbital
H_2O_2	Hydrogen peroxide
Hcy	Homocysteine
LUMO	Lowest unoccupied molecular orbital
LP	Liposome
MRI	Magnetic resonance imaging
NIR	Near-infrared
NIR-II	The second near-infrared window
NIRF	Near-infrared fluorescence imaging
$^1O_2$	Singlet oxygen
ONc	5,9,14,18,23,27,32,36-Octabutoxy-2,3-naphthalocyanine
$ONOO^-$	Peroxynitrite
$O_2^{\bullet -}$	Superoxide anion
PAI	Photoacoustic imaging
PA	Photoacoustic
PEG	Polyethylene glycol
PEG-*b*-PPG-*b*-PEG	Poly(ethylene glycol)-*b*-poly(propylene glycol)-*b*-poly (ethylene glycol)
PET	Positron emission tomography
RONS	Reactive oxygen and nitrogen species
RSS	Reactive sulfur species
RS^-	Thiolates
S_1	First excited state
S/N	Signal-to-noise ratio
TPB	Triphenyl borane
US	Ultrasound imaging
i.v.	Intravenous injection
s.c.	Subcutaneous injection
oral	Oral administration

Conflicts of interest

There are no conflicts to declare.

Acknowledgements

This work was financially supported by the National Key R&D Program of China (2020YFA0908800), National Natural Science Foundation of China (82071985), the Basic Research Program of Shenzhen (JCYJ20200109105620482, JCYJ20180507182413022), and the Shenzhen Science and Technology Program (KQTD20190929172538530). We thank the Instrumental Analysis Center of Shenzhen University (Lihu Campus).

Notes and references

1 K. L. Kirk, *Biochemistry of the elemental halogens and inorganic halides*, Springer Science & Business Media, Plenum Pre., New York, 1991.
2 M. Kleerekoper, The role of fluoride in the prevention of osteoporosis, *Endocrinol. Metab. Clin. North Am.*, 1998, **27**, 441–452.
3 K. Kaur, R. Saini, A. Kumar, V. Luxami, N. Kaur, P. Singh and S. Kumar, Chemodosimeters: An approach for detection and estimation of biologically and medically relevant metal ions, anions and thiols, *Coord. Chem. Rev.*, 2012, **256**, 1992–2028.
4 B. C. Dickinson and C. J. Chang, Chemistry and biology of reactive oxygen species in signaling or stress responses, *Nat. Chem. Biol.*, 2011, **7**, 504–511.
5 H. Sies, C. Berndt and D. P. Jones, Oxidative stress, *Annu. Rev. Biochem.*, 2017, **86**, 715–748.
6 A. J. Shuhendler, K. Pu, L. Cui, J. P. Uetrecht and J. Rao, Real-time imaging of oxidative and nitrosative stress in the liver of live animals for drug-toxicity testing, *Nat. Biotechnol.*, 2014, **32**, 373–380.
7 D. Cheng, Y. Pan, L. Wang, Z. Zeng, L. Yuan, X. Zhang and Y.-T. Chang, Selective visualization of the endogenous peroxynitrite in an inflamed mouse model by a mitochondria-targetable two-photon ratiometric fluorescent probe, *J. Am. Chem. Soc.*, 2017, **139**, 285–292.
8 W. Li, L. Wang, S. Yin, H. Lai, L. Yuan and X. Zhang, Engineering a highly selective probe for ratiometric imaging of H_2Sn and revealing its signaling pathway in fatty liver disease, *Chem. Sci.*, 2020, **11**, 7991–7999.

9 Y. Lv, D. C. Dan Cheng, D. S. Dongdong Su, M. Chen, B.-C. Yin, L. Yuan and X.-B. Zhang, Visualization of oxidative injury in the mouse kidney using selective superoxide anion fluorescent probes, *Chem. Sci.*, 2018, **9**, 7606–7613.
10 S.-H. Park, N. Kwon, J.-H. Lee, J. Yoon and I. Shin, Synthetic ratiometric fluorescent probes for detection of ions, *Chem. Soc. Rev.*, 2020, **49**, 143–179.
11 J.-F. Li, J. R. Anema, T. Wandlowski and Z.-Q. Tian, Dielectric shell isolated and graphene shell isolated nanoparticle enhanced Raman spectroscopies and their applications, *Chem. Soc. Rev.*, 2015, **44**, 8399–8409.
12 H.-H. Han, H. Tian, Y. Zang, A. C. Sedgwick, J. Li, J. L. Sessler, X.-P. He and T. D. James, Small-molecule fluorescence-based probes for interrogating major organ diseases, *Chem. Soc. Rev.*, 2021, **50**, 9391–9429.
13 K. Pu, A. J. Shuhendler, J. V. Jokerst, J. Mei, S. S. Gambhir, Z. Bao and J. Rao, Semiconducting polymer nanoparticles as photoacoustic molecular imaging probes in living mice, *Nat. Nanotechnol.*, 2014, **9**, 233–239.
14 K. Tanaka, *Handbook of in vivo chemistry in mice*, Wiley, 2020.
15 G. Rong, E. E. Tuttle, A. Neal Reilly and H. A. Clark, Recent developments in nanosensors for imaging applications in biological systems, *Annu. Rev. Anal. Chem.*, 2019, **12**, 109–128.
16 S. Zackrisson, S. M. W. Y. van de Ven and S. S. Gambhir, Light in and sound out: emerging translational strategies for photoacoustic imaging, *Cancer Res.*, 2014, **74**, 979–1004.
17 Y. Liu, L. Teng, B. Yin, H. Meng, X. Yin, S. Huan, G. Song and X.-B. Zhang, Chemical design of activatable photoacoustic probes for precise biomedical applications, *Chem. Rev.*, 2022, **122**, 6850–6918.
18 A. Taruttis and V. Ntziachristos, Advances in real-time multispectral optoacoustic imaging and its applications, *Nat. Photonics*, 2015, **9**, 219–227.
19 X. Zhang, C. Jiang, T. He, F. Zhao, J. Qu, P. Huang and J. Lin, Engineering Molecular Probes for In vivo near-infrared fluorescence/photoacoustic duplex imaging of human neutrophil elastase, *Anal. Chem.*, 2022, **94**, 3227–3234.
20 X. Zhang, K. Jiang, S. Jiang, F. Zhao, P. Chen, P. Huang and J. Lin, In vivo near-infrared fluorescence/ratiometric photoacoustic duplex imaging of lung cancer-specific hNQO1, *Anal. Chem.*, 2022, **94**, 13770–13776.
21 L. Nie and X. Chen, Structural and functional photoacoustic molecular tomography aided by emerging contrast agents, *Chem. Soc. Rev.*, 2014, **43**, 7132–7170.
22 Y. Mantri, T. R. Dorobek, J. Tsujimoto, W. F. Penny, P. S. Garimella and J. V. Jokerst, Monitoring peripheral hemodynamic response to changes in blood pressure via photoacoustic imaging, *Photoacoustics*, 2022, **26**, 100345.
23 H. J. Knox and J. Chan, Acoustogenic Probes: A new frontier in photoacoustic imaging, *Acc. Chem. Res.*, 2018, **51**, 2897–2905.
24 J. Huang and K. Pu, Activatable molecular probes for second near-infrared fluorescence, chemiluminescence, and photoacoustic imaging, *Angew. Chem., Int. Ed.*, 2020, **59**, 11717–11731.
25 X.-P. Fan, W. Yang, T.-B. Ren, S. Xu, X.-Y. Gong, X.-B. Zhang and L. Yuan, Engineering a ratiometric photoacoustic probe with a hepatocyte-specific targeting ability for liver injury imaging, *Anal. Chem.*, 2022, **94**, 1474–1481.
26 X. Liu, X. Gong, J. Yuan, X. Fan, X. Zhang, T. Ren, S. Yang, R. Yang, L. Yuan and X.-B. Zhang, Dual-stimulus responsive near-infrared reversible ratiometric fluorescent and photoacoustic probe for in vivo tumor imaging, *Anal. Chem.*, 2021, **93**, 5420–5429.
27 J. Zhang, L. Ning, Z. Zeng and K. Pu, Development of second near-infrared photoacoustic imaging agents, *Trends Chem.*, 2021, **3**, 305–317.
28 R. E. Borg and J. Rochford, Molecular Photoacoustic contrast agents: design principles & applications, *Photochem. Photobiol.*, 2018, **94**, 1175–1209.
29 M. Vogel, W. Rettig, U. Fiedeldei and H. Baumgärtel, Non-radiative deactivation via biradicaloid charge-transfer states in oxazine and thiazine dyes, *Chem. Phys. Lett.*, 1988, **148**, 347–352.
30 M. D. Laramie, M. K. Smith, F. Marmarchi, L. R. McNally and M. Henary, Small molecule optoacoustic contrast agents: An unexplored avenue for enhancing in vivo imaging, *Molecules*, 2018, **23**, 2766.
31 C. J. Reinhardt and J. Chan, Development of photoacoustic probes for in vivo molecular imaging, *Biochemistry*, 2018, **57**, 194–199.
32 M. Frenette, M. Hatamimoslehabadi, S. Bellinger-Buckley, S. Laoui, J. La, S. Bag, S. Mallidi, T. Hasan, B. Bouma, C. Yelleswarapu and J. Rochford, Shining light on the dark side of imaging: Excited state absorption enhancement of a bis-styryl BODIPY photoacoustic contrast agent, *J. Am. Chem. Soc.*, 2014, **136**, 15853–15856.
33 L. Tapia, M. Suazo, C. Hödar, V. Cambiazo and M. González, Copper exposure modifies the content and distribution of trace metals in mammalian cultured cells, *Biometals*, 2003, **16**, 169–174.
34 Y. Liu, L. Teng, H. W. Liu, C. Xu, H. Guo, L. Yuan, X. B. Zhang and W. Tan, Recent advances in organic-dye-based photoacoustic probes for biosensing and bioimaging, *Sci. China: Chem.*, 2019, **62**, 1275–1285.
35 L. Zeng, G. Ma, J. Lin and P. Huang, Photoacoustic probes for molecular detection: Recent advances and perspectives, *Small*, 2018, **14**, 1800782.
36 X. Huang, J. Song, B. C. Yung, X. Huang, Y. Xiong and X. Chen, Ratiometric optical nanoprobes enable accurate molecular detection and imaging, *Chem. Soc. Rev.*, 2018, **47**, 2873–2920.
37 Q. Fu, R. Zhu, J. Song, H. Yang and X. Chen, Photoacoustic imaging: Contrast agents and their biomedical applications, *Adv. Mater.*, 2018, **31**, 1805875.
38 Y. Wu, F. Zeng, Y. Zhao and S. Wu, Emerging contrast agents for multispectral optoacoustic imaging and their biomedical applications, *Chem. Soc. Rev.*, 2021, **50**, 7924–7940.
39 Y. Jiang and K. Pu, Advanced photoacoustic imaging applications of near-infrared absorbing organic nanoparticles, *Small*, 2017, **13**, 1700710.

40 A. K. Yadav, S. Hernandez, S. Su and J. Chan, Acoustic-based chemical tools for profiling the tumor microenvironment, *Curr. Opin. Chem. Biol.*, 2020, **57**, 114–121.
41 H.-B. Cheng, Y. Li, B. Z. Tang and J. Yoon, Assembly strategies of organic-based imaging agents for fluorescence and photoacoustic bioimaging applications, *Chem. Soc. Rev.*, 2020, **49**, 21–31.
42 G. Kim, Y.-E. K. Lee, H. Xu, M. A. Philbert and R. Kopelman, Nanoencapsulation method for high selectivity sensing of hydrogen peroxide inside live cells, *Anal. Chem.*, 2010, **82**, 2165–2169.
43 Y. Ma, L. Xu, B. Yin, J. Shang, F. Chen, J. Xu, Z. Song, B. Nan, G. Song and X. Zhang, Ratiometric semiconducting polymer nanoparticle for reliable photoacoustic imaging of pneumonia-induced vulnerable atherosclerotic plaque *in vivo*, *Nano Lett.*, 2021, **21**, 4484–4493.
44 J. Zhang, X. Zhen, P. K. Upputuri, M. Pramanik, P. Chen and K. Pu, Activatable photoacoustic nanoprobes for *in vivo* ratiometric imaging of peroxynitrite, *Adv. Mater.*, 2017, **29**, 1604764.
45 J. Zhang, X. Zhen, J. Zeng and K. Pu, A dual-modal molecular probe for near-infrared fluorescence and photoacoustic imaging of peroxynitrite, *Anal. Chem.*, 2018, **90**, 9301–9307.
46 T. Ikeno, K. Hanaoka, S. Iwaki, T. Myochin, Y. Murayama, H. Ohde, T. Komatsu, T. Ueno, T. Nagano and Y. Urano, Design and synthesis of an activatable photoacoustic probe for hypochlorous acid, *Anal. Chem.*, 2019, **91**, 9086–9092.
47 H.-W. Liu, H. Zhang, X. Lou, L. Teng, J. Yuan, L. Yuan, X.-B. Zhang and W. Tan, Imaging of peroxynitrite in drug-induced acute kidney injury with a near-infrared fluorescence and photoacoustic dual-modal molecular probe, *Chem. Commun.*, 2020, **56**, 8103–8106.
48 J. Zheng, Q. Zeng, R. Zhang, D. Xing and T. Zhang, Dynamic-reversible photoacoustic probe for continuous ratiometric sensing and imaging of redox status *in vivo*, *J. Am. Chem. Soc.*, 2019, **141**, 19226–19230.
49 X. Qin, F. Li, Y. Zhang, G. Ma, T. Feng, Y. Luo, P. Huang and J. Lin, *In vivo* photoacoustic detection and imaging of peroxynitrite, *Anal. Chem.*, 2018, **90**, 9381–9385.
50 C. Yin, X. Zhen, Q. Fan, W. Huang and K. Pu, Degradable semiconducting oligomer amphiphile for ratiometric photoacoustic imaging of hypochlorite, *ACS Nano*, 2017, **11**, 4174–4182.
51 Y. Yue, F. Huo and C. Yin, The chronological evolution of small organic molecular fluorescent probes for thiols, *Chem. Sci.*, 2021, **12**, 1220–1226.
52 C.-X. Yin, K.-M. Xiong, F.-J. Huo, J. C. Salamanca and R. M. Strongin, Fluorescent probes with multiple binding sites for the discrimination of Cys, Hcy, and GSH, *Angew. Chem., Int. Ed.*, 2017, **56**, 13188–13198.
53 A. Wang, Q. Mao, M. Zhao, S. Ye, J. Fang, C. Cui, Y. Zhao, Y. Zhang, Y. Zhang, F. Zhou and H. Shi, pH/reduction dual stimuli-triggered self-assembly of NIR theranostic probes for enhanced dual-modal imaging and photothermal therapy of tumors, *Anal. Chem.*, 2020, **92**, 16113–16121.
54 H. Fang, Y. Chen, Y. Wang, S. Geng, S. Yao, D. Song, W. He and Z. Guo, A dual-modal probe for NIR fluorogenic and ratiometric photoacoustic imaging of Cys/Hcy *in vivo*, *Sci. China Chem.*, 2020, **63**, 699–706.
55 C. Yin, F. Huo, J. Zhang, R. Martínez-Máñez, Y. Yang, H. Lv and S. Li, Thiol-addition reactions and their applications in thiol recognition, *Chem. Soc. Rev.*, 2013, **42**, 6032.
56 Z. Zhao, C. B. Swartchick and J. Chan, Targeted contrast agents and activatable probes for photoacoustic imaging of cancer, *Chem. Soc. Rev.*, 2022, **51**, 829–868.
57 Y. Zhang, J. Fang, S. Ye, Y. Zhao, A. Wang, Q. Mao, C. Cui, Y. Feng, J. Li, S. Li, M. Zhang and H. Shi, A hydrogen sulphide-responsive and depleting nanoplatform for cancer photodynamic therapy, *Nat. Commun.*, 2022, **13**, 1685.
58 T. Ma, J. Zheng, T. Zhang and D. Xing, Ratiometric photoacoustic nanoprobes for monitoring and imaging of hydrogen sulfide in vivo, *Nanoscale*, 2018, **10**, 13462–13470.
59 T. Liu, Y. Yue, Y. Zhai, Z. Guo, W. Zhao, X. Yang, D. Chen and C. Yin, Host–guest type multiple site fluorescent probe for GSH detection in living organisms, *Chem. Commun.*, 2021, **57**, 13764–13767.
60 Y. Yue, T. Zhao, K. Ma, F. Huo and C. Yin, Endogenous cysteine fluorescence monitoring and its deployment in tumour demarcation, *Chem. Commun.*, 2022, **58**, 2311–2314.
61 Y. Huang, Y. Zhang, F. Huo, J. Chao and C. Yin, A dual-targeted organelles SO_2 specific probe for bioimaging in related diseases and food analysis, *Chem. Eng. J.*, 2022, **433**, 133750.
62 R. M. Duke, E. B. Veale, F. M. Pfeffer, P. E. Kruger and T. Gunnlaugsson, Colorimetric and fluorescent anion sensors: an overview of recent developments in the use of 1,8-naphthalimide-based chemosensors, *Chem. Soc. Rev.*, 2010, **39**, 3936.
63 L. Zeng, Y. Yuan, C. Jiang, J. Mu, F. Li, Y. Wan, H. Xu, J. Qu, P. Huang and J. Lin, A near-infrared turn-on probe for in vivo chemoselective photoacoustic detection of fluoride ion, *Dyes Pigm.*, 2019, **165**, 408–414.
64 X. Huang, J. Song, B. C. Yung, X. Huang, Y. Xiong and X. Chen, Ratiometric optical nanoprobes enable accurate molecular detection and imaging, *Chem. Soc. Rev.*, 2018, **47**, 2873–2920.
65 C. Kim, C. Favazza and L. V. Wang, In Vivo Photoacoustic Tomography of Chemicals: High-resolution functional and molecular optical imaging at new depths, *Chem. Rev.*, 2010, **110**, 2756–2782.
66 W. Sun, M. Li, J. Fan and X. Peng, Activity-based sensing and theranostic probes based on photoinduced electron transfer, *Acc. Chem. Res.*, 2019, **52**, 2818–2831.
67 S. Wang and X. Zhang, Design Strategies of photoacoustic molecular probes, *ChemBioChem*, 2021, **22**, 308–316.
68 B. Du, M. Yu and J. Zheng, Transport and interactions of nanoparticles in the kidneys, *Nat. Rev. Mater.*, 2018, **3**, 358–374.
69 P. Cheng and K. Pu, Molecular imaging and disease theranostics with renal-clearable optical agents, *Nat. Rev. Mater.*, 2021, **6**, 1095–1113.

